SIMULATION OF UNSTEADY AERODYNAMIC LOAD FOR RIGID COAXIAL ROTOR IN FORWARD FLIGHT WITH VORTEX PARTICLE METHOD

Jianfeng Tan and Yiming Sun
School of Mechanical and Power Engineering, Nanjing Tech University, Nanjing 211816, R.P. China
George N. Barakos
CFD Laboratory, School of Engineering, University of Glasgow, Glasgow G12 8QQ, UK

ABSTRACT

Co-axial rotor systems are frequently used for high-speed helicopters. Nevertheless, issues related to rotor-head drag, aerodynamic performance and vibration should also be considered. Simulating the unsteady aerodynamic loads for a rigid coaxial rotor, including the aerodynamic interactions between rotors and rotor blades, is an essential part of analyzing their vibration characteristics. In this paper, an unsteady aerodynamic analysis based on the vortex-lattice method is presented. In this method, a reversed flow model on the retreating side of the coaxial rotor is proposed based on the unsteady panel method. To account for reversed flow, shedding a vortex from the leading-edge is used rather than from the trailing-edge. Moreover, vortex-blade aerodynamic interactions are modelled. The model considers the unsteady pressure term induced on a blade by tip vortices of other blades, and thus accounts for the aerodynamic interaction between the rotors and its contribution to the unsteady airloads. Coupling the reversed flow model and the vortex-blade aerodynamic interaction model with a viscous vortex particle method is used to simulate the complex wake of the coaxial rotor, closing the loop in modelling aerodynamic interactions of coaxial rotors. Following this, the unsteady aerodynamic loads on the X2 coaxial rotor are simulated in forward flight, and compared with the results of PRASADUM (Parallelized Rotorcraft Analysis for Simulation And Design, developed at the University of Maryland) and CFD/CSD computations with the OVERFLOW and the CREATE-AV Helios tools. The results of the present method agree with the results of the CFD/CSD method, and compare better than the PRASADUM solutions. Furthermore, the influence of the aerodynamic interaction between the coaxial rotors on the unsteady airloads, frequency, wake structure, induced flow and force distributions are analyzed. Additionally, the results are also compared against computation for a single rotor case, simulated at similar conditions as the coaxial rotor. It is shown that the effect of tip vortex interaction plays a significant role in unsteady airloads of coaxial rotors at low-speeds, while the rotor blade passing effect is obvious strengthened at high-speed.

1. INTRODUCTION

Coaxial rotor systems, such as XH-59A and X2, receive nowadays increased attention as emphasis is placed on high speed platforms [1,2]. Blade stall has been one of the main factors limiting the speed of single main rotor helicopters, and the coaxial rotor can eliminate this by off-loading the retreating blade as the advancing blades generate the necessary lift and maintain roll balance. However, like single rotors, coaxial rotors produce vortex-dominated wakes that play a significant role in the performance of rotorcraft. Furthermore, their wake is much more complex than the wake of single rotor because the two rotors and their wakes interact with one another [3]. In addition, the aerodynamic interference between the upper and lower rotors is a significant factor that needs to be considered for coaxial rotor systems. These interactions can result in vibratory hub loads creating undesirable handling qualities and acoustics. The unsteady loads for the coaxial rotor were found to be at least an order of magnitude larger than the single isolated rotor under same conditions [4]. Moreover, the rotors are

subjected in much larger vibratory bending stresses in flight than would occur for articulated rotors of similar size [5]. Therefore, increased vibratory loads are one of the disadvantages of a coaxial rotor configuration, and achieving acceptable vibration levels and handling qualities without adding significant parasitic weight is a challenge [2]. Since unsteadiness in the aerodynamic load is a major source of vibration, understanding the unsteady aerodynamics of the coaxial rotor system in forward flight is essential to analyze their vibration.

Numerical simulations, including computationally efficient vortex-lattice methods and high-fidelity Computational Fluid Dynamics (CFD) simulations, have greatly contributed to the advancement of the aeromechanics of coaxial rotors. Past CFD studies aimed to obtain a deep understanding of the unsteady aerodynamic loads characteristics of rotors, and were often coupled with Computational Structural Dynamics (CSD) to understand the vibratory loads and affect rotor design parameters, such as rotor spacing, stiffness, lift offset, and clocking [4, 6]. However, the unsteady aerodynamic predictions of a coaxial rotor by CFD are affected by several factors such as the need for high-density grids to capture the rotor wake, and the associated computational cost in finding just one solution is considerable. Therefore, aerodynamic analysis of the coaxial rotors with less computational effort, remains one of the most challenging tasks of the CFD community. Vortex-lattice methods (VLM) are seen as an alternative to grid-based CFD, and are attractive because they require less computational effort. For this reason, VLM have recently received significant attention in the literature.

The vortex-lattice methods, including free-wake methods [7], Vorticity Transport Models (VTM) [8], and Vortex particle methods (VPM) [9, 10], are a powerful approach to simulating complex rotor wakes. Such methods are ideally suited to propagating vortices over long distances and offer an efficient flow description and can be easily coupled with CSD to analyze control loads needed for rotor design. Therefore, this method was adopted by tools such as CHARM [2], to simulate the performance of a coaxial rotor, and was also coupled with comprehensive tools, such as CARMRADII [11], UMARC [1], RCAS [12], PRASADUM [4] to investigate the vibratory loads of coaxial rotors in forward flight. However, there are significant factors to be investigated, such as blade-wake interactions, reversed flow, vortex shedding from leading-edge [13].

An unsteady aerodynamic analysis method based on vortex particle method and including the effect of the reversed flow and blade-vortex interaction is developed to simulate the complex wake of the coaxial rotor. In this approach, the reversed flow model on the retreating side of the coaxial rotor is proposed based on the unsteady panel method. Shedding a vortex from the leading-edge on the retreating side is used, rather than shedding from the trailing-edge to account for the effect of the flow reversal. Furthermore, the effect of vortex-blade aerodynamic interaction is modelled by considering the unsteady pressure term induced on a blade by tip vortices of other blades, and thus accounts for the aerodynamic interaction between the dual-rotors and its contribution to the unsteady airloads.

2. COMPUTATIONAL METHOD

2.1 Aerodynamic Model of Coaxial Rotor

A model of the X2 Technology Demonstrator (X2TD) is modeled in the present work based on data from public-domain information [13-16]. This main rotor blade was designed to mitigate large drag experienced by the inboard sections in reversed flow with double ended elliptic sections, while a high-lift cross-section is used at mid-span, which transitions to a transonic airfoil at the tip to reduced compressibility drag. The distribution of airfoil cross-sections, such as DBLN-526, SC1012-R8, SSCA-09, are then adopted, and the construction of the upper and lower rotors are identical in the present work. Also, to ensure the blade geometry matched as closely as possible to available data, the sections of blades are interpolated to ensure smoothness along the blade surface. Base on the unsteady panel method, the blade of X2 is modeled as smooth surface grid shown in Fig.1.

The aerodynamic model of the coaxial rotor blades is firstly represented using an unsteady panel method [10]. Based on this method, a velocity potential ϕ is defined as

(1) $$\phi(x,y,z,t)=\frac{1}{4\pi}\int_{S_B}\mu\boldsymbol{n}\cdot\nabla(\frac{1}{r})dS-\frac{1}{4\pi}\int_{S_B}\sigma(\frac{1}{r})dS+\frac{1}{4\pi}\int_{S_w}\mu\boldsymbol{n}\cdot\nabla(\frac{1}{r})dS$$

where σ and μ are the source and doublet distributions placed on the blade and wake surfaces, $\boldsymbol{n}$ denotes the outward unit normal vector of a surface, and $\boldsymbol{r}$ is the position vector (x, y, z).

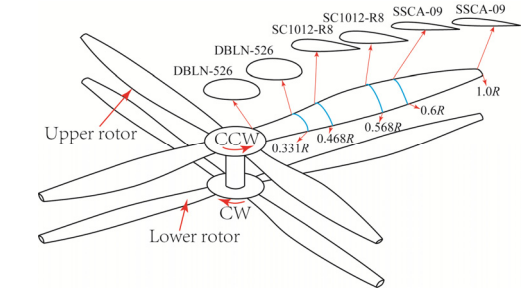

(a) Airfoil distribution

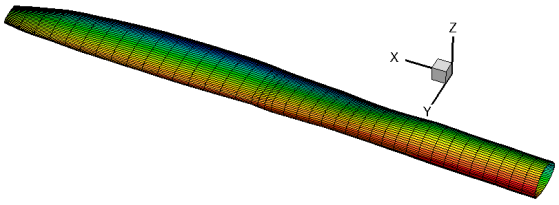

(b) Grid of blade

Fig.1 Airfoil and grid of the coaxial rotor

The boundary condition for the blade surfaces requires that the velocity component normal to S_B to be zero. A boundary condition of infinity requires the flow disturbance to decrease far away from the rotor owing to the blade's motion through fluid. The boundary condition can then be expressed as

(2) $$\begin{cases}\dfrac{\partial\phi}{\partial n}-\boldsymbol{v}_B\cdot\boldsymbol{n}=0 & \text{blade surface}\\ \lim\nabla\phi_{r\to\infty}=0 & \text{infinite boundary}\end{cases}$$

where $\boldsymbol{v}_B$ is the velocity of a point on blade surface S_B and $\boldsymbol{n}$ denotes the outward unit normal vector at this point. Moreover, $\boldsymbol{r}$ is the position vector (x, y, z). The infinite boundary condition is automatically fulfilled through Green's function.

2.2 Reversed Flow Model

In the aerodynamic model of single rotor blade based on an unsteady panel method, the wake shedding from the trailing-edge of airfoil at all azimuth locations, including the retreating side, is modeled with the trailing-edge Kutta condition. The model is suitable to represent the aerodynamics of rotor blade, this is because of the fact that the reversed flow is limited in a small area on the retreating side due to limited maximum forward speed and has weak influence on the aerodynamic airloads in the single rotor. However, as the flight speed increases, the reversed flow on the retreating side of both upper and lower rotor of coaxial rotor system may expand to 0.5R. Also, as opposed to the single rotor, flow attachment on the retreating side of the coaxial rotor system is observed. As a result, the blade section corresponding to the reversed flow also produces some lift, and can be modeled by the panel method. Additionally, the vortex shedding from the reversed flow will interact with other blades of the upper and lower rotor resulting in unsteadiness of aerodynamic loads for coaxial rotor system. Therefore, a reversed flow model is taken into account and coupled into the aerodynamic model of coaxial rotor in the present work.

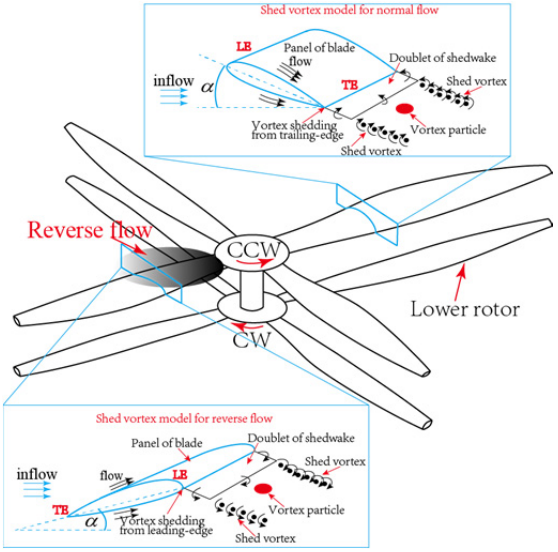

Fig.2 Reversed flow model of coaxial rotor system

It is assumed that the flow convects from leading-edge to trailing-edge on the advancing side, and the Kutta condition at trailing-edge is satisfied. Therefore, wake doublets can be expressed in terms of the unknown surface doublet through the trailing-edge Kutta condition. Defining upper and lower trailing edge (T.E.) doublets as μ_u^{TE} and μ_d^{TE}, respectively, the T.E. wake doublet μ_w^{TE} is given as

(3) $$\mu_w^{TE}=\mu_u^{TE}-\mu_d^{TE}$$

However, as opposed to the advancing side, the vortex

shed from leading edge in the reversed flow on the retreating side of coaxial rotor. Because of the flow attachment on the retreating side, it is assumed that the leading-edge Kutta condition is satisfied, as shown in Fig.2. Therefore, the wake doublets can be expressed in terms of the unknown surface doublet through a leading-edge Kutta condition. Defining the upper and lower leading edge (L.E.) doublets as μ_u^{LE} and μ_d^{LE}, respectively, the L.E. wake doublet μ_w^{LE} is given as

(4) $$\mu_w^{LE} = \mu_u^{LE} - \mu_d^{LE}$$

The potential inside the blade (without internal singularities) will not change for an enclosed boundary (e.g. S_B). Therefore, the internal potential is set to $\phi_{\text{int}} = 0$.

(5) $$\frac{1}{4\pi}\int_{S_B} \mu \boldsymbol{n}\cdot\nabla(\frac{1}{r})dS - \frac{1}{4\pi}\int_{S_B}\sigma(\frac{1}{r})dS + \frac{1}{4\pi}\int_{S_w}\mu\boldsymbol{n}\cdot\nabla(\frac{1}{r})dS = 0$$

By dividing the coaxial rotor blade surface into N panels and wake surface into N_w panels, integration on the surfaces in Eq. (5) can be equivalently written as the superposition of integrations on the panels that constitute those surfaces. Quadrilateral geometry, constant-strength panels are adopted in the current study. Thus, Eq. (5) can be rewritten as

(6) $$\sum_{k=1}^{N}\mu_k A_k = -\sum_{k=1}^{N}\sigma_k B_k$$

where A_k includes contributions of the blade surface as well as of the rotor wake surface, and A_k and B_k can be solved by the analytic formulations for a constant strength of potential distribution on each panel. The A_k is given as

(7) $$A_k = \begin{cases} \frac{1}{4\pi}\int_{\text{blade}} \mathbf{n}_k\cdot\nabla(1/|\mathbf{r}_k|)\mathrm{d}s_{\text{k}} & k \neq LE \text{ or } TE \\ \frac{1}{4\pi}\int_{\text{blade}} \mathbf{n}_k\cdot\nabla(1/|\mathbf{r}_k|)\mathrm{d}s_{\text{k}} \pm \frac{1}{4\pi}\int_{TE\ wake}\mathbf{n}_{TE}\cdot\nabla(1/|\mathbf{r}_{TE}|)\mathrm{d}s_{\text{TE}} & k = TE \\ \frac{1}{4\pi}\int_{\text{blade}} \mathbf{n}_k\cdot\nabla(1/|\mathbf{r}_k|)\mathrm{d}s_{\text{k}} \pm \frac{1}{4\pi}\int_{LE\ wake}\mathbf{n}_{LE}\cdot\nabla(1/|\mathbf{r}_{LE}|)\mathrm{d}s_{\text{LE}} & k = LE \end{cases}$$

(8) $$B_k = -\frac{1}{4\pi}\int_{\text{blade}}(1/|\mathbf{r}_k|)\mathrm{d}s_{\text{k}}$$

The conversion of doublet panels at leading-edge to vortex wake in the reversed flow is realized following the coupled method in Ref.10 that the flow induced by a dipole surface distribution μ defined on a surface S is equivalent to a surface term involving surface vorticity $\gamma = \boldsymbol{n}\times\nabla\mu$ and a line vortex term μ over the boundary of the surface. A collection of vortex wake in the surface centre is obtained by integrating the surface vorticity $\gamma = \boldsymbol{n}\times\nabla\mu$ throughout the wake panel and the line vortex μ bounding the surface.

2.3 Effect of Vortex-Blade Aerodynamic Interaction

The interaction of the upper rotor wake with lower rotor, along with that between tip vortices from the two rotors with each other and the inboard sheet, produce a highly complicated flow-field and unsteadiness of airloads. Consequently, the unsteady effect of coaxial rotor wake should to be taken into account in prediction of airloads. Base on the panel method as mentioned before, the unsteady pressure on the blade surfaces can be calculated by using the velocity potential and flow velocity through the Bernoulli equation.

(9) $$\frac{\partial\phi}{\partial t} + \frac{1}{2}\boldsymbol{v}^2 + \frac{1}{\rho}p = \frac{1}{\rho}p_{\text{ref}}$$

The vortex of the upper rotors impinges on the blade surface of the lower rotor resulting in variation of the unsteady term $\partial\phi/\partial t$ in Eq.(9) and the unsteady pressure response, especially for blade vortex interaction (BVI). It is believed that the interaction between the coaxial-rotor systems plays a significant role in the amount of unsteadiness of the airloads, and should be taken into account in prediction of the time-varying airloads. Therefore, the effect of vortex-blade aerodynamic interaction is modelled thought the unsteady pressure term induced by the coaxial-rotor wake and both rotor blades. Thus, the non-dimensionalised form of the blade unsteady pressure is then given as

(10) $$C_p^{\text{u}} = \frac{p^{\text{u}} - p_{\text{ref}}}{(1/2)\rho(\boldsymbol{v}_{\text{ref}}^{\text{u}})^2} = 1 - \frac{(\boldsymbol{v}_{\text{B}}^{\text{u}})^2}{(\boldsymbol{v}_{\text{ref}}^{\text{u}})^2} - \frac{2}{(\boldsymbol{v}_{\text{ref}}^{\text{u}})^2}(\frac{\partial\phi_{\text{b}}^{\text{l}}}{\partial t} + \frac{\partial\phi_{\text{w}}^{\text{l}}}{\partial t})$$

$$C_p^{l} = \frac{p^{\text{l}} - p_{\text{ref}}}{(1/2)\rho(\boldsymbol{v}_{\text{ref}}^{\text{l}})^2} = 1 - \frac{(\boldsymbol{v}_{\text{B}}^{\text{l}})^2}{(\boldsymbol{v}_{\text{ref}}^{\text{l}})^2} - \frac{2}{(\boldsymbol{v}_{\text{ref}}^{\text{l}})^2}(\frac{\partial\phi_{\text{b}}^{\text{u}}}{\partial t} + \frac{\partial\phi_{\text{w}}^{\text{u}}}{\partial t})$$

where p_{ref} and ρ are far-field reference pressure and density, $\boldsymbol{v}_{\text{B}}^{\text{u}}$, p^{u}, $\boldsymbol{v}_{\text{ref}}^{\text{u}}$ are the local fluid velocity, local pressure, reference velocity, respectively, at each section of the upper rotor, while $\boldsymbol{v}_{\text{B}}^{\text{l}}$, p^{l}, $\boldsymbol{v}_{\text{ref}}^{\text{l}}$ are the local fluid velocity, local pressure, reference velocity, respectively, at each section of the lower rotor. Also, $\phi_{\text{b}}^{\text{u}}$ and $\phi_{\text{w}}^{\text{u}}$ are the velocity potential induced by the upper rotor blades

and its wake, respectively, whereas $\phi_{\mathrm{b}}^{\mathrm{l}}$ and $\phi_{\mathrm{w}}^{\mathrm{l}}$ are the velocity potential induced by the lower rotor blades and its wake, respectively.

The unsteady pressure term induced by both rotor blades can be directly described by the derivative of velocity potential, whilst that of the coaxial-rotor wake can be transformed into the product of induced velocity from wake and velocity of wake (induced velocity from vortex particles and velocity of vortex particles), which is similar to the effect of tip-vortex filaments [17]. Those derivatives of velocity potential can be expressed as

$$\partial\phi_{\mathrm{b}}^{\mathrm{u}}/\partial t=(\phi_{\mathrm{b}}^{\mathrm{u},t}-\phi_{\mathrm{b}}^{\mathrm{u},t-\Delta t})/\Delta t \qquad \partial\phi_{\mathrm{b}}^{\mathrm{l}}/\partial t=(\phi_{\mathrm{b}}^{\mathrm{l},t}-\phi_{\mathrm{b}}^{\mathrm{l},t-\Delta t})/\Delta t \tag{11}$$

$$\partial\phi_{\mathrm{w}}^{\mathrm{u}}/\partial t=-\sum \boldsymbol{v}_{\mathrm{ind}}^{\mathrm{u}}(\boldsymbol{x}_{\mathrm{u}})\cdot\boldsymbol{v}_{\mathrm{w}}^{\mathrm{l}}(\boldsymbol{x}_{\mathrm{l}}') \qquad \partial\phi_{\mathrm{w}}^{\mathrm{l}}/\partial t=-\sum \boldsymbol{v}_{\mathrm{ind}}^{\mathrm{l}}(\boldsymbol{x}_{\mathrm{l}})\cdot\boldsymbol{v}_{\mathrm{w}}^{\mathrm{u}}(\boldsymbol{x}_{\mathrm{u}}') \tag{12}$$

where $\boldsymbol{x}_{\mathrm{u}}$, $\boldsymbol{v}_{\mathrm{w}}^{\mathrm{u}}$, $\boldsymbol{x}_{\mathrm{u}}'$ are blade position, velocity and position of tip vortex of the upper rotor, respectively, while $\boldsymbol{x}_{\mathrm{l}}$, $\boldsymbol{v}_{\mathrm{w}}^{\mathrm{l}}$, $\boldsymbol{x}_{\mathrm{l}}'$ are blade position, velocity and position of tip vortex of the lower rotor, respectively. $\boldsymbol{v}_{\mathrm{ind}}^{\mathrm{u}}$ and $\boldsymbol{v}_{\mathrm{ind}}^{\mathrm{l}}$ are velocity of the upper rotor induced by the lower rotor tip vortex and velocity of the lower rotor induced by the upper rotor tip vortex, respectively.

The aerodynamic airloads on the panels of both the upper and lower rotor can be then computed as

$$\Delta\boldsymbol{F}_k=-C_{pk}\left(\rho\boldsymbol{v}_{\mathrm{ref}}^2/2\right)_k\Delta S_k\boldsymbol{n}_k \tag{13}$$

where $\Delta\boldsymbol{F}_k$ is the aerodynamic load on the panel, ΔS_k is the panel area, and $\boldsymbol{n}_{\mathrm{k}}$ is its normal vector.

2.4 Wake Model of the Coaxial-Rotor System

The vortex shedding from the coaxial-rotor system may directly induce unsteady pressure response and twist the rotor tip vortex. Therefore, simulating the coaxial rotor wake plays a significant role in prediction of unsteady airloads of the coaxial-rotor system. The wake of the coaxial-rotor system shown in Fig.3 is depicted base on a viscous vortex particle method[10] which solves the Navier-Stokes equation with velocity-vorticity ($\boldsymbol{u}$, $\boldsymbol{\omega}$) in Lagrangian frame by using vector-valued particles.

$$\frac{\partial\boldsymbol{\omega}}{\partial t}+\boldsymbol{u}\cdot\nabla\boldsymbol{\omega}=\nu\nabla^2\boldsymbol{\omega}+\nabla\boldsymbol{u}\cdot\boldsymbol{\omega} \tag{14}$$

The right hand-side term describes vortex particle convection which is solved by using a fourth-order Runge-Kutta scheme, and the left hand-side term expresses the viscous diffusion and stretching effect. The viscous diffusion effect is simulated through particle strength exchange (PSE), and the vortex stretching effect is represented by a direct scheme.

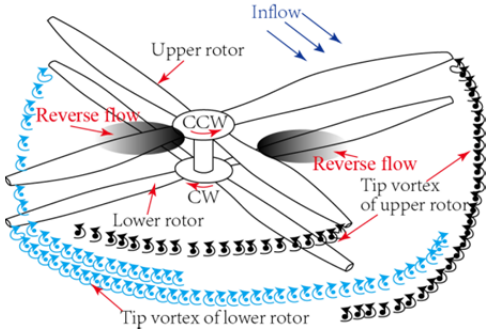

Fig.3 Tip vortex of coaxial rotor

The trailing-edge vortex and leading-edge vortex are shed from the surface of the coaxial rotor blade through Neumann boundary condition and by converting shed-wake doublet panels to wake vorticity. After then, it convects based on Eq.(14).

3 NUMERICAL RESULTS AND DISCUSSSION

3.1 Unsteady Airloads of Coaxial-Rotor System

The X2TD model is computed in forward flight. This coaxial rotor has eight blades with non-uniform chord and non-linear twist. The rotor radius is 4.023m and the tip Mach number is 0.554. The airfoil distribution with DBLN-526, SC1012-R8, SSCA-09 scheme is shown in Fig.1. The blade is modelled with 19200 panels composed of 60 panels in the chordwise direction and 40 panels in the spanwise direction. The azimuthal angle step is 2.5°.

Figure 4 shows the variation in the sectional thrust coefficient at characteristic radial stations over one revolution at different flight speeds, μ=0.15, 0.27, and 0.41. Note that, when viewed from above, the upper rotor rotates in an anti-clockwise fashion and the lower rotor rotates clockwise. Therefore, to clearly plot and compare the variation of the sectional airloads, the azimuthal locations of the upper and lower rotors are measured in the rotational direction of the upper rotor. The results are also compared with result of PRASADUM and full grid-based CFD results [13]. In the PRASADUM solver,

blade section aerodynamics based on a lifting-line method was modelled using look-up tables with quasi-steady and non-circulatory corrections for airfoil pitch and plunge motions. Also, two inflow models, finite-state dynamic inflow and Maryland free wake, were integrated into the solver to account for the influence of the coaxial-rotor wake. The CFD solvers of the CREATE AV Helios framework include OVERFLOW, and overset meshes can be used to simulate aerodynamic interactions.

The variations of the sectional thrust coefficient at different flight speeds in the present simulation correlate well with those found in the CFD results of Helios near the azimuthal angles of 60° and 300°. Furthermore, the thrust coefficient is also in accordance with CFD results in terms of magnitude and phase. Additionally, the influence of the interaction between the coaxial rotor wake and the blades on the sectional thrust distributions is observed on the advancing side at azimuthal angles of around 40-120° and on the retreating side at around 260-320°. The present predictions and the results of PRASADUM show similar trends as the CFD result at different flight speeds. However, at low speed flight, the unsteady airloads are under-predicted by PRASADUM on the advancing side at azimuthal angles of around 40-120° and on the retreating side at around 260-320°, while at high speed flight, over-prediction occur. Moreover, the airloads of the lower rotor were also over-predicted at different flight speeds. Therefore, compared with the PRASADUM result, the predicted fluctuations of sectional thrust is agree better with the CFD result on the advancing side at azimuthal angles of around 40-120° and on the retreating side at around 260-320°. It should be noted that even though there are some discrepancies in the present prediction, the overall comparison is still good and the results of the present method are found to match well with the results of the CFD/CSD method.

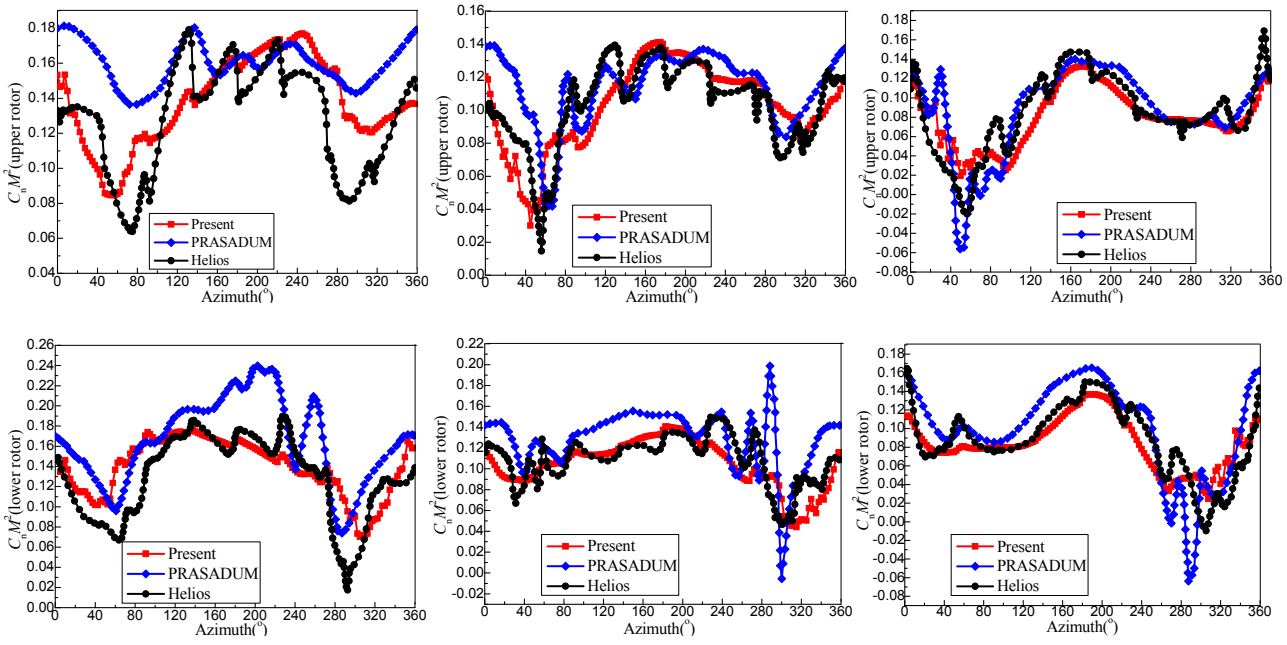

(a) μ=0.15 (b) μ=0.27 (c) μ=0.41

Fig.4 Sectional airloads of coaxial rotor at different forward speeds

3.2 Differential Aerodynamic Loads Between the Upper and Lower rotor

The azimuthal distribution of unsteady airloads on the upper and lower rotor in Figure 5 provides some insight into the difference of the airloads on the coaxial rotor blades. Comparing the airloads of the upper rotor at low forward speed, we can see that the airloads of the lower rotor reduce visible on the advancing side at azimuthal angles of around 40-120° and on the retreating side at around 260-320°, especially at an azimuthal angle of 300°. This is a result of the interaction between the wakes of the coaxial rotor blades. Additionally, as expected, the tip vortex of the upper rotor impinges on the lower rotor as shown in Fig.6. Note that in this graph, the tip vortex of the upper rotor is indicated with red, while the tip vortex of the

lower rotor is indicated with blue. Moreover, the lower rotor blade on the advancing side at azimuthal angles of around 40-120° and on the retreating side around 260-320° are affected by the rolled-up tip vortex, interpreted as super-vortices, of the upper rotor which results in decrease of the angle of attack.

As flight speed increases, the difference of airloads between the upper and lower rotor decreases as shown in Fig.5. This is because, the rotor wake at high advance ratio is swept away quickly and the angle of attack between the upper and lower rotors is quite similar. In addition, it is observed in Fig.6 that the tip vortex of upper rotor swept above the lower rotor result in weakening interaction between the upper and lower rotor wake.

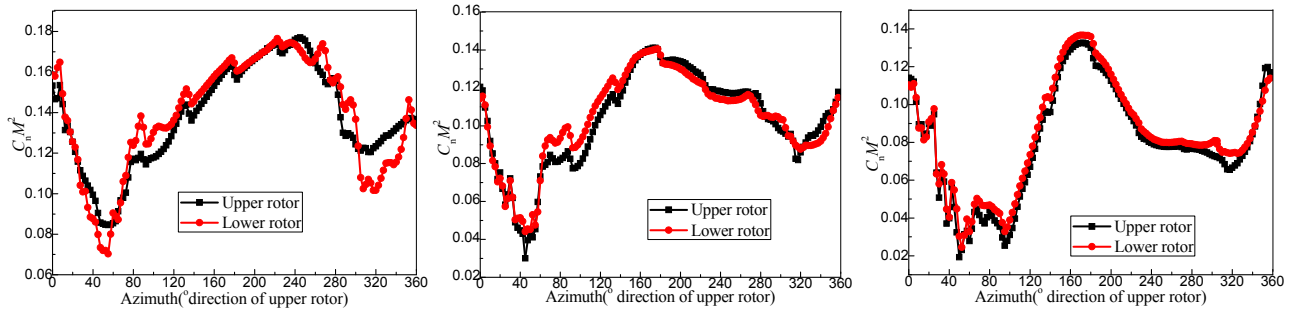

(a) μ=0.15 (b) μ=0.27 (c) μ=0.41

Fig.5 Sectional airload of the upper and lower rotor

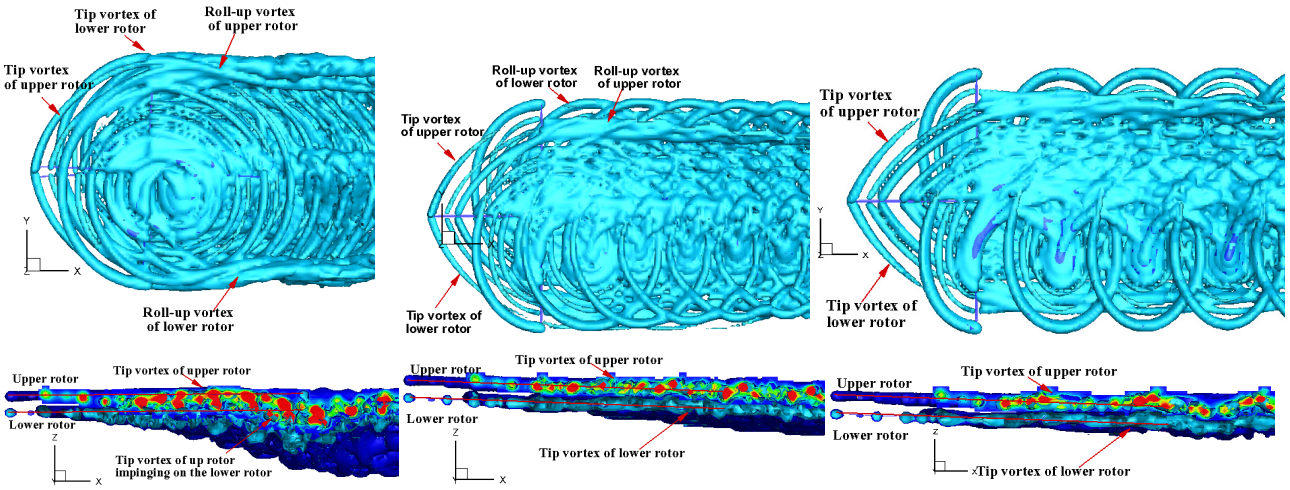

(a) μ=0.15 (b) μ=0.27 (c) μ=0.41

Fig.6 Rotor wake of coaxial rotor at different forward speeds

The distributed inflows of the upper and lower rotor at two different forward speeds, μ=0.15 and 0.41, are shown in Fig.7. As mentioned before, the rotor wake at low speed convects down and impinges on the lower rotor resulting in reduction of inflow on the advancing side at azimuthal angles of 40-120° and on the retreating side at 260-320°. As a result, the blade vortex interaction is obvious on the advancing side at azimuthal angles of around 40-120° and on the retreating side at around 260-320° which is shown in Fig.7(c). However, the difference of inflow between the upper and lower rotor decreases as the flight speed increases. Also, the reduced inflow due to blade vortex interaction disappears, and the influence of vortex interaction between the upper and lower rotor is alleviated as the rotor wake swept away quickly.

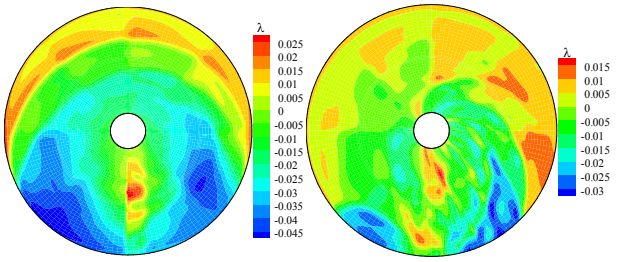

(a) Upper rotor(μ=0.15) (d) Upper rotor(μ=0.41)

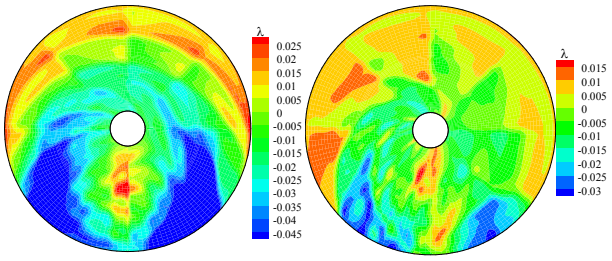

(b) Lower rotor(μ=0.15) (e) Lower rotor(μ=0.41)

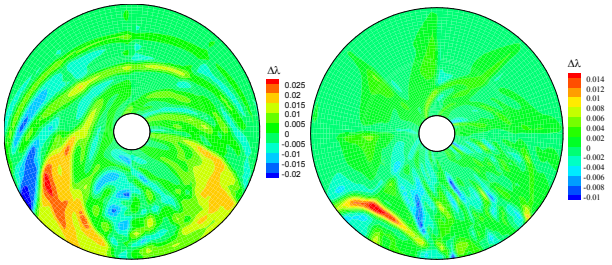

(c) Difference(μ=0.15) (f) Difference(μ=0.41)

Fig.7 Induced velocity of coaxial rotor

Figure 8 describes the distribution of force for the upper and lower rotor at two different forward speeds. At low speed forward, the area of reversed flow is small and the lift off-set is also limited, therefore, the forces in the forward and backward parts of the rotor plan are obvious and shown in Fig.8a and Fig.8b. Moreover, it is worth noting that in this graph, the difference in forces between the upper and lower rotors is striped on the advancing and retreating side due to the tip vortex of the upper rotor impinging on the lower rotor as mentioned earlier. This fluctuation of forces indicates the influence of blade-vortex interaction on the coaxial rotor system. In addition, the differences in force on the retreating side at the azimuth of 260-320° is most important because of the obvious reduction of inflow induced by the tip vortex of the upper rotor.

As the flight speed increases, the reversed flow expands and the lift off-set increases, as a result, the force on the advancing side is the dominant component of rotor thrust for both the upper and lower rotor. Furthermore, with increasing speed, the difference of force on the advancing and retreating side due to the tip vortex interaction between the upper and lower rotor decreases, while the difference of force corresponding to the effect of blade passage increases. It can be seen that the difference in force shows 8/rev unsteady loads. This is because both the upper and lower rotor wakes move downstream quickly, resulting in weakened interaction between the coaxial rotor system. However, as the blades of the upper and lower rotor approach each other, each blade induces an upwash on the other blade. The upwash increases as the blades approach each other, but after a certain point it begins to decrease, and changes sign acting as a downwash. The strength of the downwash is seen to initially increase and then starts decreasing as the blades move away from each other. Correspondingly, the forces on both the upper and lower rotor increase as the blades approach, then decrease and then increase again as they move away.

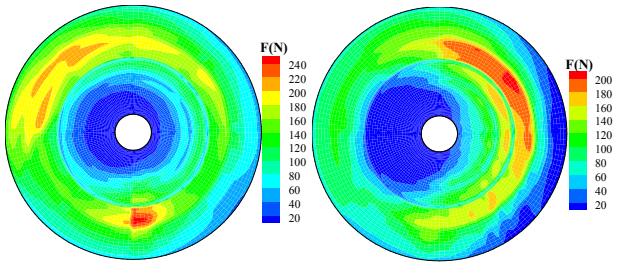

(a) Upper rotor(μ=0.15) (d) Upper rotor(μ=0.41)

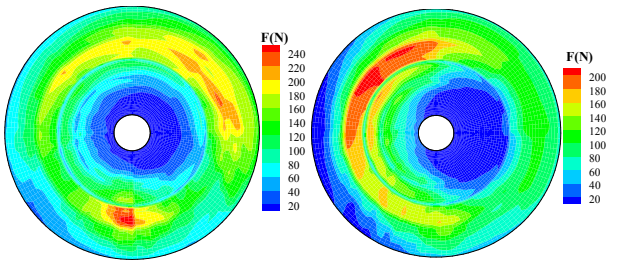

(b) Lower rotor(μ=0.15) (e) Lower rotor(μ=0.41)

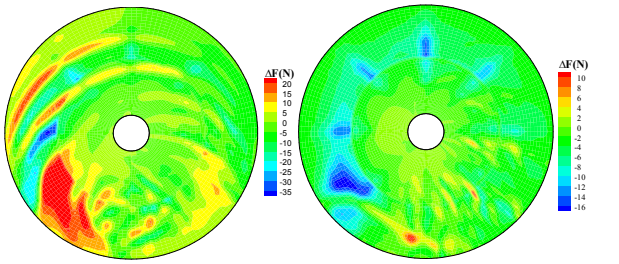

(c) Difference(μ=0.15) (f) Difference(μ=0.41)

Fig.8 Sectional force of coaxial rotor

The wake visualization of the coaxial rotor at low speed, μ=0.15, is shown in Fig.9. The iso-surface is coloured by the sense of the vorticity vector. Similar to the single rotor, the tip vortices trailing behind the blades tangle around one another and roll up along the rotor on the advancing and retreating sides, and the fully rolled-up vorticity structure is well defined and discrete. The fully rolled-up vorticity structure is similar to the tip vortex observed

behind a single rotor and fixed-wing aircraft. However, it is interest to note that the tip vortices from the upper and lower rotor blades interact with each other and produce two coherent rolled-up bundles. At the first instance, the tip vortex of the upper rotor, indicated as ①, is above the tip vortex of the lower rotor, indicated as ②. At a later time, the tip vortex ① shed from the upper blades contracts in the radial direction and convects down owing to the induced velocity of the lower rotor tip vortex ② at x=0.5R-0.75R result in the upper rotor wake structure impinging on the lower rotor, while the tip vortex ② is pushed upstream due to induced effect of the upper rotor tip vortex ①. As a result, the tip vortex ② comes to contact with the tip vortex ① under their mutually-induced effect and the tip vortex ① changes position with the tip vortex ② resulting in two coherent rolled-up bundles. Moreover, it is also observed that the tip vortex of the upper rotor contracts faster in the radial direction compared to that of the lower rotor caused by the influence of roll-up vortex of the lower rotor.

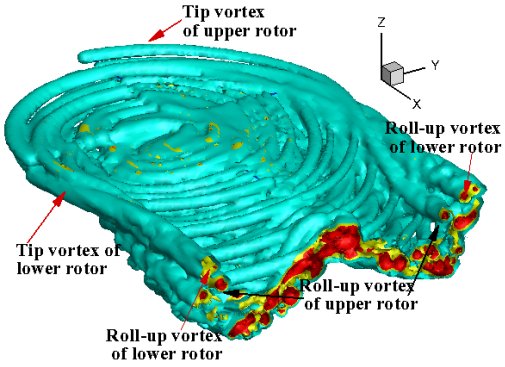

(a) Wake structure

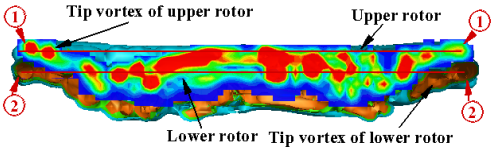

(b) x=0.25R

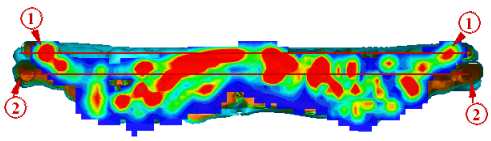

(c) x=0.5R

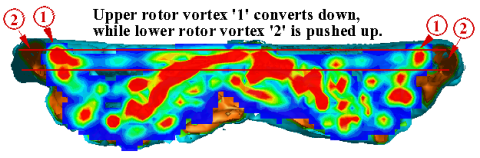

(d) x=0.75R

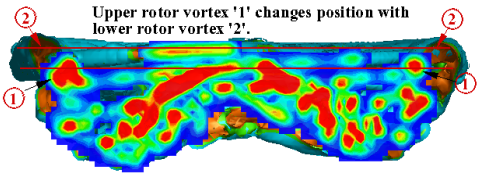

(e) x=1.0R

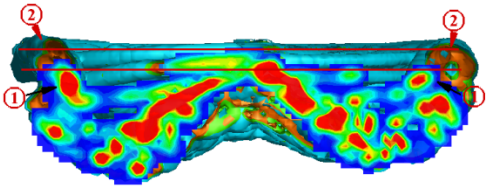

(f) x=1.25R

Fig.9 Interchange of tip vortex position of coaxial rotor (μ=0.15)

The azimuthal distribution and frequency of induced flow and sectional thrust coefficient at a radial station, r/R=0.75, in Figure 10 provides insight into the effect of the tip vortex interaction between the upper and lower rotor. The induced inflow at azimuth of 80-240° for the upper and lower rotor is similar. However, the induced inflow of the lower rotor on the advancing side at azimuth of 0-80°and on the retreating side at azimuth of 240-360° is more serious than that of the upper rotor due to tip vortex interaction of the lower rotor. Furthermore, the tip vortex interaction causes not only a 17.5% increase in the 1/rev component but also yields a 30.9%, 144.2%, 194.7% increase in the 3/rev, 4/rev, 5/rev components, respectively. In addition, the 3/rev, 4/rev, 5/rev component of unsteady airloads for the lower rotor also increase compared to that of the upper rotor.

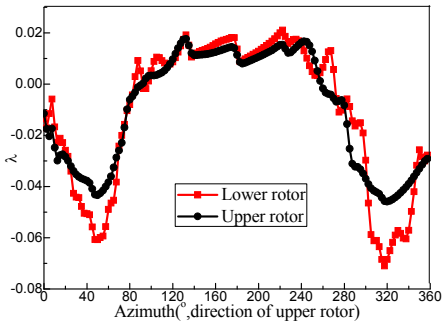

(a) Induced flow

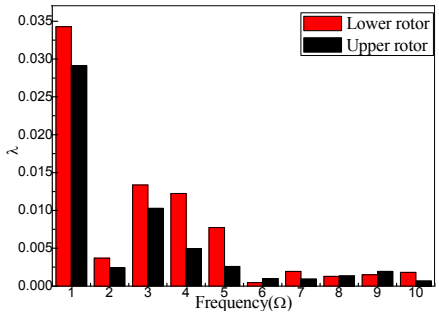

(b) Frequency of induced flow

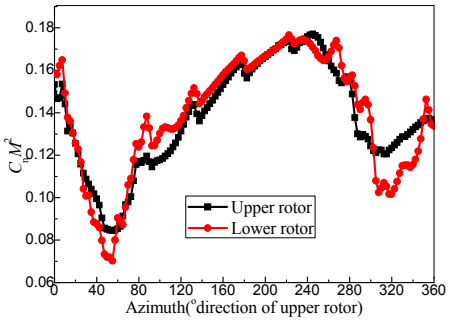

(c) airload

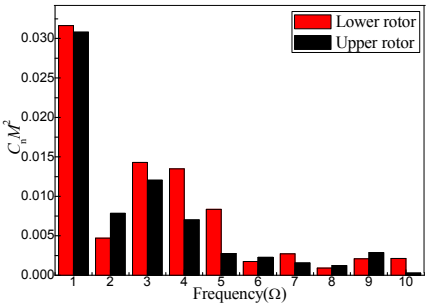

(d) Frequency of sectional airload

Fig.10 Frequency of sectional airload and induced flow of coaxial rotor (μ=0.15)

3.3 Differential Aerodynamic Loads Between Coaxial and Single rotor

Figure 11 shows the azimuthal distribution of sectional thrust coefficient for the coaxial rotor and single rotor at three flight speed. The geometry and control scheme of the single rotor are identical to the coaxial rotor to analyse the different airload in the same condition. Clearly, as opposed to the single rotor system, the sectional thrust coefficient on the advancing side at azimuthal angles of 60° and on the retreating side at 300° is obvious smaller because of the influence of the tip vortex of the other rotor. This is because the upper rotor tip vortex at low speed impinges on the lower rotor resulting in reduction of inflow on the advancing side at azimuthal angles of around 40-120° and on the retreating side at around 260-320°, while the inflow of single rotor only affected by itself tip vortex. As a result, the sectional thrust coefficient reduces. This suggests that, contrary to the single rotor system, the tip vortex interaction between the upper and lower rotor is comparable or maybe even predominant. However, the difference of sectional thrust coefficient between the coaxial rotor and single rotor decreases with increasing flight speed. This is because, the tip vortex convects downstream quickly and the mutual interaction of the upper and lower rotor is weakened.

The frequencies of sectional thrust coefficients for the coaxial and single rotors at three flight speeds are also shown in Fig.11 which shows that, contrary to the single rotor, the 1/rev, 3-10/rev components of thrust coefficient on the coaxial rotor obviously increase. However, the difference of 1/rev component decreases with increasing flight speed. The reason for the differences is explained by the tip vortex interaction on the advancing side at azimuthal angles of 60° and on the retreating side at 300° at low speed which is seen to contribute to significant increasement of the 1/rev component, while the interaction decrease as the flight speed increases. Nevertheless, as the flight speed increases, the 8/rev component of the coaxial rotor is greater than that of single rotor due to the rotor blade passing effect which induces high frequency unsteady pressure and is more obvious in high speed. For the coaxial rotor, each rotor blade of the lower rotor will meet other blades of the upper rotor 8 times, which result in 8/rev component of unsteady airloads.

Figure 12 illustrates the difference of induced flow and section force between the coaxial rotor and single rotor. The tip vortex interaction between the coaxial-rotor systems is obviously seen to generate significant fluctuation of inflow and force on the advancing and retreating side at low speed flight. In addition, the variation of blade passing effect is also can be observed due to the interaction between blades of the upper and lower rotor. However, as the flight speed increase, the effect of the tip vortex interaction of the coaxial rotor is weakened and the fluctuation on the advancing and retreating side reduce. Additionally, the variation due to blade passing effect is strengthened. Therefore, the aerodynamic interaction in the coaxial rotor is more serious than the single rotor.

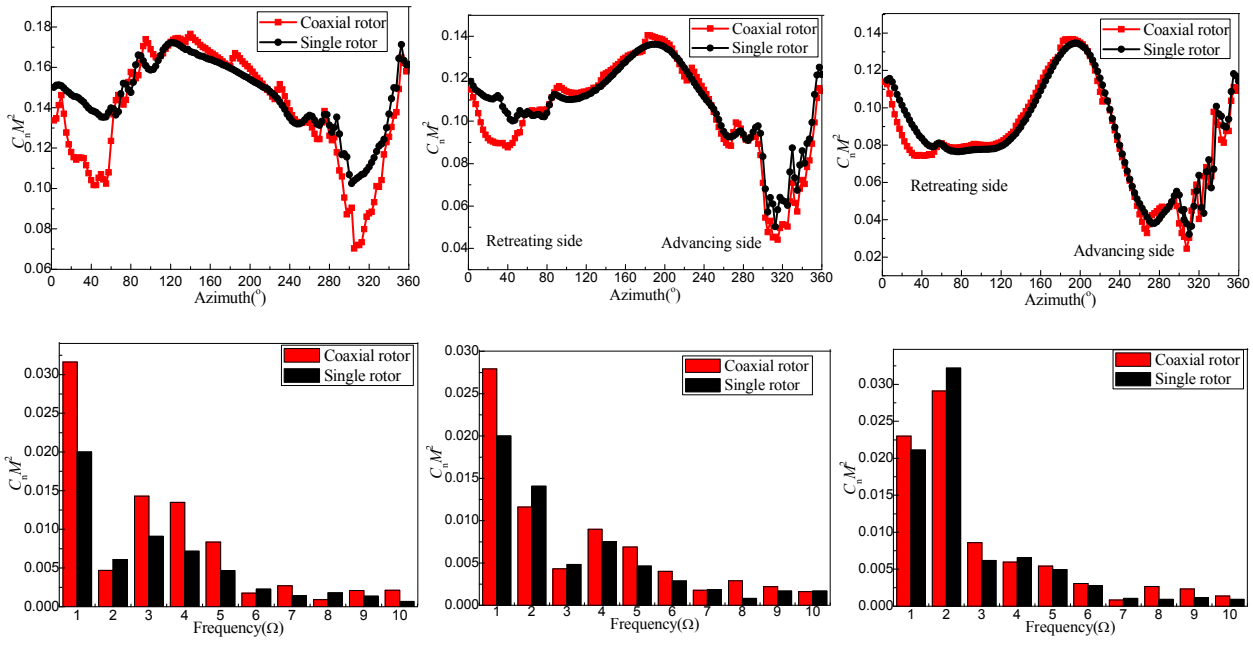

(a) μ=0.15 (b) μ=0.27 (c) μ=0.41

Fig.11 Sectional airload and frequency of coaxial and single rotor

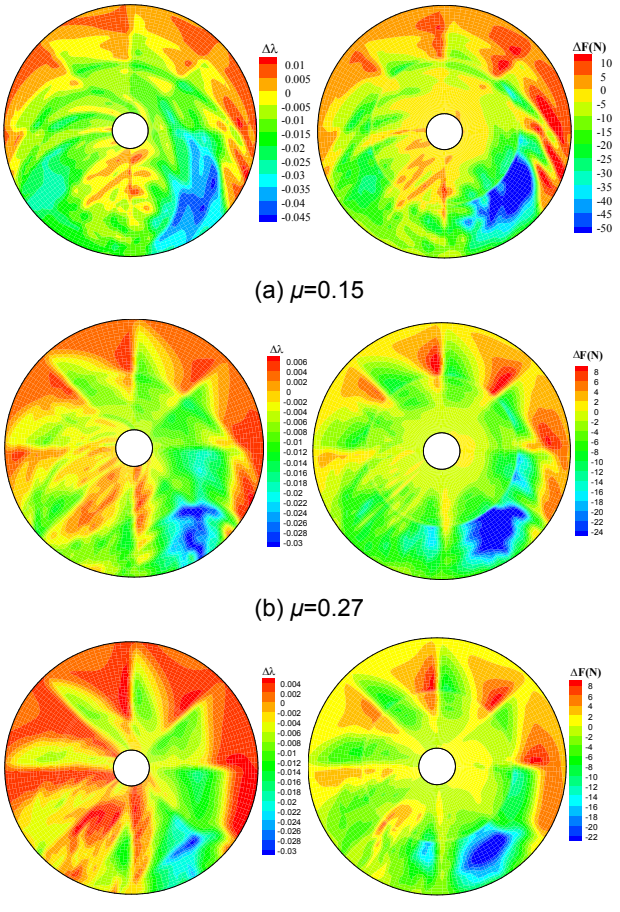

(a) μ=0.15

(b) μ=0.27

(c) μ=0.41

Fig.12 Change in induced velocity and sectional force due to single and coaxial rotor

4. CONCLUSIONS

An unsteady aerodynamic analysis method including a reversed flow model for the retreating side of the coaxial rotor, the effect of vortex-blade aerodynamic interaction, and a vortex particle method is developed to simulate the unsteady aerodynamic loads for a coaxial rotor. This includes the aerodynamic interactions between rotors and rotor blades. The unsteady aerodynamic loads on the X2 coaxial rotor are simulated in forward flight, and compared with the results of PRASADUM and published CFD/CSD computations with the OVERFLOW and the CREATE-AV Helios tools. The results of the present method agree well with the results of the CFD/CSD method, and compare better than the PRASADUM solutions. Furthermore, comparing the inflow and airloads of the upper rotor at low forward speed, the airloads of the lower rotor reduce at the advancing and retreating sides due to the tip vortex of upper rotor impinging on the lower rotor. The difference of airloads between the upper and lower rotor decreases with increasing flight speed. However, the difference of forces corresponding to the effect of the blade passage increases. Moreover, the tip vortices from the upper and lower rotor blades interact with each other and produce two coherent rolled-up bundles and change position at low speed, while the rotor wake at high advance ratio is swept

away quickly resulting in a weakened interaction between both rotors. Additionally, contrary to the single rotor system, the tip vortex interaction between the upper and lower rotor is comparable or maybe even predominant to the difference of the sectional thrust coefficient between the coaxial rotor and single rotor. However, as the flight speed increases, the inflow and airloads due to the rotor blade passing effect of coaxial rotor becomes pronounced.

ACKNOWLEGEMENTS

This work was supported by the National Natural Science Foundation of China (Grant No. 11502105), and the support of Natural Science Foundation of Jiangsu Province (Grant No. BK20161537) and the Jiangsu Government Scholarship for Overseas Studies were gratefully acknowledged.

REFERENCES

[1] Schmaus, J., Chopra, I. Aeromechanics for a High Advance Ratio Coaxial Helicopter. The AHS 71st Annual Forum, Fairfax, VA, 2015: 1139-1153

[2] Gaffey, T. M., Zhang, C., Quackenbush, D. T., Sheng, C. H., Hasbun, M. Aeromechanics of the Coaxial Compound Helicopter. 56th AIAA/ASCE/AHS/ASC Structures, Structural Dynamics, and Materials Conference, Reston, VA, AIAA, 2015.

[3] Mula, S. M., Cameron, C. G., Tinney, C. E., Sirohi, J. Low-dimensional Characteristics of Tip Vortices From a Coaxial Rotor in Hover. AHS 70th Annual Forum and Technology Display, Montreal, Canada, 2014.

[4] Singh, R., Kang, H. Computational Investigations of Transient Loads and Blade Deformations on Coaxial Rotor Systems. 33rd AIAA Applied Aerodynamics Conference, Reston, VA, AIAA, 2015.

[5] Eller, E. X2TM Load Alleviating Controls. The American Helicopter Society 68th Annual Forum, Fairfax, VA, AHS, 2012.

[6] Singh, R., Kang, H., Bhagwat, M., Cameron, C., Sirohi, J. Computational and Experimental Study of Coaxial Rotor Steady and Vibratory Loads. 54th AIAA Aerospace Sciences Meeting, Reston, VA, AIAA, 2016.

[7] Syal, M., Leishman, J.G. Aerodynamic Optimization Study of a Coaxial Rotor. Presented at 65th Annual Forum of the American Helicopter Scociety, Grapevine, TX, 2009.

[8] Kim, H. W., Brown, R. E. Coaxial Rotor Performance and Wake Dynamics in Steady and Manoeuvring Flight. Presented at the American Helicopter Society 62nd Annual Forum, Phoenix, Arizona, 2006.

[9] He, C. J., Zhao, J. G. Modeling Rotor Wake Dynamics With Viscous Vortex Particle Method. AIAA Journal, 2009, 47(4): 902-915.

[10] Tan, J. F., Wang, H. W. Simulating Unsteady Aerodynamics of Helicopter Rotor with Panel/Viscous Vortex Particle Method. Aerospace Science and Technology, 2013, 30: 255-268.

[11] Yeo, H., Johnson, W. Investigation of Maximum Blade Loading Capability of Lift-offset Rotors. The AHS 69th Annual Forum, Fairfax, VA, AHS, 2013.

[12] Ho, J. C., Yeo, H., Bhagwat, M. Validation of Rotorcraft Comprehensive Analysis Performance Predictions for Coaxial Rotors in Hover. Presented at the AHS 71st Annual Forum, Virginia Beach, 2015.

[13] Passe, B., Sridharan, A., Baeder, J. Computational Investigation of Coaxial Rotor Interactional Aerodynamics in Steady Forward Flight. 33rd AIAA Applied Aerodynamics Conference, Reston, VA, AIAA, 2015.

[14] Bagai, A. Aerodynamic Design of the X2 Technology Demonstrator™ Main Rotor Blade. Presented at the 64th Annual Forum of the American Helicopter Society, Montreal, Canada, 2008.

[15] Blackwell, R., Millott, T. Dynamics Design Characteristics of the Sikorsky X2 Technology™ Demonstrator Aircraft. Presented at the American Helicopter Society 64th Annual Forum, Montreal, Canada, 2008.

[16] Walsh, D., Weiner, S., Arifian, K., Lawrence, T., Wilson, M., Millott, T., Blackwell, R. High Airspeed Testing of the Sikorsky X2 Technology™ Demonstrator. Presented at the 67th Annual Forum of the American Helicopter Society International, Virginia Beach, VA, 2011.

[17] Lorber, P. F., Egolf, T. A. An Unsteady Helicopter Rotor-fuselage Aerodynamic Interaction Analysis. Journal of the American Helicopter Society, 1990, 35(3): 32-42.